Journal of Zhejiang University-SCIENCE A (Applied Physics & Engineering) 2023 24(11):937-948
www.jzus.zju.edu.cn; www.springer.com/journal/11582
E-mail: jzus_a@zju.edu.cn

Research Article

https://doi.org/10.1631/jzus.A2200484

Core-drilling kinematic modeling and analysis of Jiaolong submersible manipulator

Xu YANG[1], Xin LIU[1], Shizhen LI[1]✉, Yugang REN[2]✉, Limin ZHU[3]

[1]*Institute of Marine Science and Technology, Shandong University, Qingdao 266237, China*
[2]*National Deep Sea Center, Qingdao 266237, China*
[3]*State Key Laboratory of Mechanical System and Vibration, Shanghai Jiao Tong University, Shanghai 200240, China*

Abstract: The complicated topographies of the deep sea pose significant challenges for the core drilling with the Jiaolong submersible manipulator. To address this problem, we proposed a core-drilling kinematic model and evaluated the core-drilling behavior of the submersible manipulator by comprehensively considering the uncertain posture of the Jiaolong submersible. First, we established a forward kinematic model for the core-drilling task in deep sea, which satisfied the requirement of gravitational-direction core drilling. Based on the forward kinematic equations, we then built a double-redundancy inverse kinematic model, which was able to determine the required motion trajectories of six active joints according to the desired core-drilling trajectory. The core-drilling workspaces and the motions of the Jiaolong submersible manipulator were assessed with several calculation examples. The established forward and inverse kinematic models are constructed with clear analytic equations, and thus are directly applicable to the Jiaolong submersible manipulator-based core-drilling task.

Key words: Kinematic model; Core drilling; Jiaolong submersible manipulator; Uncertain posture

1 Introduction

The deep sea is the last vast area on earth that has not been extensively explored and developed, and is rich in minerals, energy, medicinal substances, various forms of life, and many other natural resources (Lauro et al., 2009). Submersibles are key apparatuses for exploring, developing, and protecting the deep sea (Zhang et al., 2017). By 2018, 160 submersibles were in service around the world (Kohnen, 2018), some of which had even reached the Challenger Deep of the Mariana Trench, the Galapas Rift of the Eastern Pacific Ocean, and the Mid-Atlantic Ridge (Kohnen, 2013).

Core drilling along the gravitational direction is one important task for submersibles; it plays an important role in detecting polymetallic sulfides (Iizasa et al., 1999), gas hydrate (Khlystov et al., 2013), ferromanganese crust (Chu et al., 2005), sediment (Reagan et al., 2017), and many other resources in the deep sea. In 1991, the American ALVIN submersible successfully performed core-drilling operations at 2100-m water depth and obtained samples representing the progressive mineral growth of chimneys (Stakes et al., 1992). During the cruise of the French Nautile submersible in 1996, 66 basaltic rock samples were collected from the center of the Mid-Atlantic Ridge (Ravilly et al., 2001). The Chinese Jiaolong submersible obtained mud volcano samples from the Mariana Trench (Ren et al., 2021) and cobalt-rich crust samples from the Vega Seamount (Yao et al., 2021). The Japanese Shinkai 6500 submersible collected microplastic sediment samples from the deep-sea floor in Japanese waters (Tsuchiya et al., 2019). To accommodate the complicated topographies of the deep sea, submersibles usually operate a core-drilling rig with a multi-degree-of-freedom manipulator (Wu et al., 2014). Nevertheless, it is a challenging task to determine the right position and posture trajectories for deep-sea manipulators in order to accomplish a core-drilling operation.

✉ Shizhen LI, kmlishizhen@126.com
Yugang REN, ryg@ndsc.org.cn
Shizhen LI, https://orcid.org/0000-0003-2487-1807
Yugang REN, https://orcid.org/0000-0001-6867-6910

Received Oct. 16, 2022; Revision accepted Feb. 28, 2023;
Crosschecked Sept. 1, 2023

To solve the trajectory issues of deep-sea manipulators, much research work on kinematic modeling has been carried out. For example, Khan and Quan (2015) established a forward kinematic model for the Puma 560 underwater manipulator. Chen et al. (2021) obtained the inverse kinematic model of a 6-degree-of-freedom (DOF) underwater manipulator by using the Jacobi matrix generalized inverse method. Qiao et al. (2010) resolved the inverse kinematic equations for a general 6R serial manipulator by double quaternions. Zhang et al. (2022) proposed to solve the inverse kinematic of a deep-sea hydraulic manipulator by combining the geometric method and the Euler angles solution. Finally, Luo et al. (2022) employed a multi-objective full-parameter optimization particle swarm optimization algorithm to improve the accuracy, efficiency, and stability of inverse kinematic calculation. However, the existing research is focused on kinematic models of underwater manipulators. Manipulator-based core drilling is different and complex which involves six active joints and one passive joint. In addition, the core-drilling trajectory must be along the gravitational direction regardless of the posture of the submersible.

Motivated by the urgent needs of deep-sea core drilling, we established a functionalized kinematic model for the Jiaolong submersible manipulator in this study. We took the submersible posture and the gravitational constraint into account to build a forward kinematic model for the Jiaolong submersible manipulator-based core-drilling task. The established forward kinematic model can ensure a specific sediment-direction drilling posture by solving the angular displacement of joint 6 based on the angular displacements of joints 1–5 and the submersible posture. Furthermore, we deduced a double-redundancy inverse kinematic algorithm by means of the iterative elimination method. The trajectories in joint space can be analytically determined with the established inverse kinematic model.

The main contribution of this research lies in solving the forward and inverse problems of the Jiaolong submersible manipulator-based core-drilling task. The rest of the paper is organized as follows. The core-drilling operation of the Jiaolong submersible manipulator is introduced in Section 2. The core-drilling forward kinematic model is built in Section 3. A double-redundancy inverse kinematic model is presented in Section 4. Section 5 covers the Jiaolong submersible manipulator-based core-drilling operation simulations and analysis. Finally, conclusions are drawn in Section 6.

2 Jiaolong submersible manipulator-based core drilling

The Jiaolong submersible is the first Chinese deep-sea manned submersible and offers several unique features: a maximum operational depth of 7062 m (Cui, 2013), dimensions of 8.4 m×3.9 m×3.4 m (Zhang et al., 2016), a weight of 22 t (Liu et al., 2010), a crew of one pilot and two scientists (Zhu, 2020), and a manned cabin with an inner diameter of 2.1 m (Wang et al., 2020), as shown in Fig. 1a. The Jiaolong submersible is capable of working across 99.8% of the world's ocean area (Zhang et al., 2018). It is equipped with two seven-function manipulators that can accomplish various deep-sea tasks such as geological sampling, biological sampling, seawater sampling, and in-situ cutting (Sivčev et al., 2018). While performing core drilling of deposit sediment in the deep sea, the Jiaolong submersible manipulator is required to actuate the core-drilling rig along the gravitational direction, as shown in Fig. 1b.

(a) (b)

Fig. 1 Jiaolong manned submersible (a) and manipulator-based core drilling (b)

The Jiaolong submersible manipulator is a six-DOF serial robot with additional grasping function (Orion 7PE, Schilling Robotics, LLC, USA), as shown in Fig. 2a. Active joints 1, 2, 3, and 5 are revolute pairs driven by hydraulic cylinders. Active joints 4 and 6 are revolute pairs driven by hydraulic motors. The end-jaw is actuated by a hydraulic cylinder. In order to facilitate rapid grabbing and a constant mechanical relationship, the core-drilling rig is usually connected with the end-jaw through a passive revolute pair. As a result, passive joint 7 is a revolute pair without actuation. By controlling the angular positions of six active joints, the Jiaolong submersible manipulator can adjust the position and posture of the core-drilling rig. The key parameters of Jiaolong submersible manipulator are: 7000-m rated water depth, weight in air of 61 kg, weight in seawater of 43 kg, and 55.3-kg lift at full extension. Despite of the uncertain submersible posture, the position and posture of the core-drilling rig can be maintained by regulating the manipulator trajectory.

3 Core-drilling forward kinematic model

3.1 Posture modeling of the Jiaolong submersible

First, we established a world coordinate (w-coordinate) and a base coordinate (0-coordinate), as shown in Fig. 2b. The origins of the w-coordinate and the 0-coordinate are attached to each other. The z_w axis of the w-coordinate is arranged along the gravitational direction. The z_0 axis of the 0-coordinate is along the shaft axis of joint 1. The x_0 axis of the 0-coordinate is along the common normal line of the shaft axes of joints 1 and 2 (while the angle of joint 1 is zero). The y_0 axis of the 0-coordinate is determined with the right-hand rule. The roll-pitch-yaw (RPY) angles (Li et al., 2007; Wang et al., 2018) are used to describe the position and posture relationship between the w-coordinate and the 0-coordinate. The transformation matrix which denotes the effect of an uncertain submersible posture on the manipulator can be expressed by:

$$
\begin{aligned}
{}^{\mathrm{w}}_{0}\boldsymbol{T}(\alpha,\beta,\gamma) &= \begin{bmatrix} r_{11} & r_{12} & r_{13} & 0 \\ r_{21} & r_{22} & r_{23} & 0 \\ r_{31} & r_{32} & r_{33} & 0 \\ 0 & 0 & 0 & 1 \end{bmatrix} = \\
&\boldsymbol{T}(x_{\mathrm{w}},\gamma)\boldsymbol{T}(y_{\mathrm{w}},\beta)\boldsymbol{T}(z_{\mathrm{w}},\alpha) = \\
&\begin{bmatrix} c_\alpha c_\beta & -s_\alpha c_\beta & s_\beta & 0 \\ s_\alpha c_\gamma + c_\alpha s_\beta s_\gamma & c_\alpha c_\gamma - s_\alpha s_\beta s_\gamma & -c_\beta s_\gamma & 0 \\ s_\alpha s_\gamma - c_\alpha s_\beta c_\gamma & c_\alpha s_\gamma + s_\alpha s_\beta c_\gamma & c_\beta c_\gamma & 0 \\ 0 & 0 & 0 & 1 \end{bmatrix},
\end{aligned} \tag{1}
$$

where r_{ij} denotes the matrix element in the ith row and the jth column, $\boldsymbol{T}(x_{\mathrm{w}},\gamma)$ is the rotation-transformation matrix around the x_{w} axis, γ is the roll angle from the w-coordinate to the 0-coordinate around the x_{w} axis, $\boldsymbol{T}(y_{\mathrm{w}},\beta)$ is the rotation transformation matrix around y_{w} axis, β is the pitch angle from the w-coordinate to the 0-coordinate around the y_{w} axis, $\boldsymbol{T}(z_{\mathrm{w}},\alpha)$ is the rotation transformation matrix around z_{w} axis, and α is

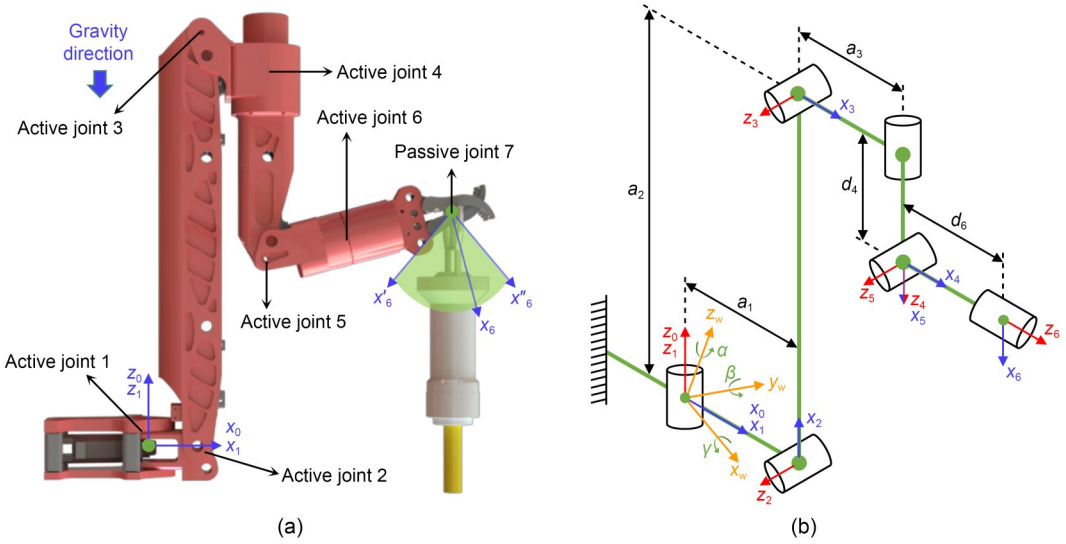

Fig. 2 Jiaolong submersible manipulator-based core drilling (a) and coordinates of Jiaolong submersible manipulator (b)

the yaw angle from the w-coordinate to the 0-coordinate around the z_w axis (Fig. 2b). s_α denotes sinα, c_α denotes cosα, and so do s_β, c_β, s_γ, and c_γ.

3.2 Jiaolong manipulator kinematic modeling

Six linkage coordinate systems $\{i\}$ (i-coordinate, i=1, 2, ⋯, 6) were established for the Jiaolong submersible manipulator, using the Denavit-Hartenberg method (Roh and Kim, 2004; Dereli and Köker, 2020; Xiao et al., 2021, Li et al., 2022), as shown in Fig. 2b. The origins of the 1-coordinate and the 0-coordinate were attached to each other. The z_1 axis of the 1-coordinate was along the z_0 axis of the 0-coordinate. The x_1 axis of the 1-coordinate was along the common normal line of the shaft axes of joints 1 and 2. The origin of the 2-coordinate was attached to joint 2. The z_2 axis of the 2-coordinate was along the shaft axis of joint 2. The x_2 axis of the 2-coordinate was along the common normal line of the shaft axes of joints 2 and 3. The origin of the 3-coordinate was attached to joint 3 and the z_3 axis of the 3-coordinate was along the shaft axis of joint 3. The x_3 axis of the 3-coordinate was along the common normal line of the shaft axes of joints 3 and 4. The origin of the 4-coordinate was attached to joint 4. The z_4 axis of the 4-coordinate was along the shaft axis of joint 4. The x_4 axis of the 4-coordinate was along the cross-product direction of z_5 and z_4. The origin of the 5-coordinate was attached to joint 5. The z_5 axis of the 5-coordinate was along the shaft axis of joint 5. The x_5 axis of the 5-coordinate was along the cross-product direction of z_6 and z_5. The origin of the 6-coordinate was attached to the manipulator's end-jaw. The z_6 axis of the 6-coordinate was along the shaft axis of joint 6. The x_6 axis of the 6-coordinate was parallel to the x_5 axis of the 5-coordinate. To describe the geometrical relationship between various linkages, we defined link parameters a_{i-1}, α_{i-1}, d_i, and θ_i (i=1, 2, ⋯, 6). a_{i-1} is the length of link $i-1$, α_{i-1} is the angle from z_{i-1} to z_i around x_{i-1} axis, d_i is the distance from x_{i-1} to x_i along z_i axis, and θ_i is the angle from x_{i-1} to x_i around z_i axis. The kinematic transformation matrix from the 0-coordinate to the 6-coordinate of the Jiaolong manipulator is:

$$ {}^0_6\boldsymbol{T}={}^0_1\boldsymbol{T}\,{}^1_2\boldsymbol{T}\,{}^2_3\boldsymbol{T}\,{}^3_4\boldsymbol{T}\,{}^4_5\boldsymbol{T}\,{}^5_6\boldsymbol{T}=\begin{bmatrix} n_x & o_x & a_x & p_x \\ n_y & o_y & a_y & p_y \\ n_z & o_z & a_z & p_z \\ 0 & 0 & 0 & 1 \end{bmatrix}, \quad (2) $$

where ${}^{i-1}_i\boldsymbol{T}$ is the transformation matrix from $(i-1)$-coordinate to i-coordinate (i=1, 2, ⋯, 6), n_x, n_y, n_z, o_x, o_y, o_z, a_x, a_y, and a_z denote the posture elements of the manipulator's end-jaw in the 0-coordinate, and p_x, p_y, and p_z denote the position elements of the manipulator's end-jaw in the 0-coordinate.

3.3 Core-drilling forward kinematic modeling

Taking the posture of the Jiaolong submersible into account, the transformation matrix from the w-coordinate to the 6-coordinate is:

$$ \begin{aligned} {}^w_6\boldsymbol{T}&={}^w_0\boldsymbol{T}\,{}^0_6\boldsymbol{T}=\begin{bmatrix} r_{11} & r_{12} & r_{13} & 0 \\ r_{21} & r_{22} & r_{23} & 0 \\ r_{31} & r_{32} & r_{33} & 0 \\ 0 & 0 & 0 & 1 \end{bmatrix}\begin{bmatrix} n_x & o_x & a_x & p_x \\ n_y & o_y & a_y & p_y \\ n_z & o_z & a_z & p_z \\ 0 & 0 & 0 & 1 \end{bmatrix}= \\ &\begin{bmatrix} r_{11}n_x+r_{12}n_y+r_{13}n_z & r_{11}o_x+r_{12}o_y+r_{13}o_z \\ r_{21}n_x+r_{22}n_y+r_{23}n_z & r_{21}o_x+r_{22}o_y+r_{23}o_z \\ r_{31}n_x+r_{32}n_y+r_{33}n_z & r_{31}o_x+r_{32}o_y+r_{33}o_z \\ 0 & 0 \end{bmatrix} \\ &\begin{bmatrix} r_{11}a_x+r_{12}a_y+r_{13}a_z & r_{11}p_x+r_{12}p_y+r_{13}p_z \\ r_{21}a_x+r_{22}a_y+r_{23}a_z & r_{21}p_x+r_{22}p_y+r_{23}p_z \\ r_{31}a_x+r_{32}a_y+r_{33}a_z & r_{31}p_x+r_{32}p_y+r_{33}p_z \\ 0 & 1 \end{bmatrix}. \end{aligned} \quad (3) $$

Eq. (3) indicates the position and posture of the manipulator's end-jaw in the w-coordinate. To ensure that the shaft axis of the core-drilling rig is along the gravitational direction (z_w axis of the w-coordinate), the y_6 axis of the 6-coordinate should be parallel to the x_w–y_w plane of the w-coordinate (because the core-drilling rig is attached to the end-jaw by means of a passive revolute pair). Herein, the following constraint equation can be derived:

$$ {}^w_6T(3,\,2)=r_{31}o_x+r_{32}o_y+r_{33}o_z=0. \quad (4) $$

By substituting the elements o_x, o_y, and o_z into Eq. (4), the constraint equation can be rewritten as:

$$ {}^w_6T(3,\,2)=c_6g_x+s_6g_y=0, \quad (5) $$

$$ g_x=r_{31}(c_1c_{23}s_4-s_1c_4)+r_{32}(s_1c_{23}s_4+c_1c_4)+r_{33}s_4s_{23}, \quad (6) $$

$$ g_y=r_{31}(c_1s_{23}s_5-c_1c_{23}c_4c_5-s_1s_4c_5)+r_{32}(s_1s_{23}s_5-s_1c_{23}c_4c_5+c_1s_4c_5)-r_{33}(s_5c_{23}+c_4c_5s_{23}), \quad (7) $$

where s_i denotes $\sin\theta_i$ (i=1, 2, ⋯, 6), c_i denotes $\cos\theta_i$ (i=1, 2, ⋯, 6), θ_i (i=1, 2, ⋯, 6) denotes the joint variable of the ith joint, s_{ij} denotes $\sin(\theta_i+\theta_j)$, and c_{ij} denotes $\cos(\theta_i+\theta_j)$.

By using trigonometrical substitution, Eq. (5) can be rewritten as:

$$\sqrt{g_x^2+g_y^2}\cos\left[\mathrm{Atan2}\left(g_y,\ g_x\right)-\theta_6\right]=0. \tag{8}$$

From Eq. (8), the analytical solution of θ_6 can be obtained as:

$$\theta_6=\psi(\theta_1,\ \theta_2,\ \theta_3,\ \theta_4,\ \theta_5)=\begin{cases}\forall, & g_x=0\wedge g_y=0,\\ \mathrm{Atan2}\left(g_y,\ g_x\right)-\arccos(0), & g_x\neq 0\vee g_y\neq 0.\end{cases} \tag{9}$$

By substituting the analytical solution of θ_6 (Eq. (9)) into the kinematic transformation matrix Eq. (2), the elements of a core-drilling forward kinematic model can be obtained as:

$$\begin{cases}
n_x=s_\psi(c_1c_{23}s_4-s_1c_4)-\\
\quad c_\psi(c_1s_{23}s_5-c_1c_{23}c_4c_5-s_1s_4c_5),\\
n_y=s_\psi(s_1c_{23}s_4+c_1c_4)-\\
\quad c_\psi(s_1s_{23}s_5-s_1c_{23}c_4c_5+c_1s_4c_5),\\
n_z=s_\psi s_4s_{23}+c_\psi(s_5c_{23}+c_4c_5s_{23}),\\
o_x=c_\psi(c_1c_{23}s_4-s_1c_4)+\\
\quad s_\psi(c_1s_{23}s_5-c_1c_{23}c_4c_5-s_1s_4c_5),\\
o_y=c_\psi(s_1c_{23}s_4+c_1c_4)+\\
\quad s_\psi(s_1s_{23}s_5-s_1c_{23}c_4c_5+c_1s_4c_5),\\
o_z=c_\psi s_4s_{23}-s_\psi(s_5c_{23}+c_4c_5s_{23}),\\
a_x=-c_5c_1s_{23}-s_5(c_1c_{23}c_4+s_1s_4),\\
a_y=-c_5s_1s_{23}-s_5(s_1c_{23}c_4-c_1s_4),\\
a_z=c_5c_{23}-c_4s_5s_{23},\\
p_x=a_1c_1+a_2c_1c_2+a_3c_1c_{23}+d_4c_1s_{23}-\\
\quad d_6(c_1c_{23}c_4s_5+s_1s_4s_5+c_1s_{23}c_5),\\
p_y=a_1s_1+a_2s_1c_2+a_3s_1c_{23}+d_4s_1s_{23}-\\
\quad d_6(s_1c_{23}c_4s_5-c_1s_4s_5+s_1s_{23}c_5),\\
p_z=a_2s_2+a_3s_{23}-d_4c_{23}-d_6(s_{23}c_4s_5-c_{23}c_5),
\end{cases} \tag{10}$$

where s_ψ denotes $\sin\psi$, and c_ψ denotes $\cos\psi$.

4 Core-drilling inverse kinematic model

Based on the established core-drilling forward kinematic model of the Jiaolong submersible manipulator, we built a double-redundancy inverse kinematic model in this section. Given the core-drilling position (the tip position of the core-drilling rig in the w-coordinate) $[W_x\ W_y\ W_z]^{\mathrm{T}}$ and the length of core-drilling rig L_1, the following formulas can be obtained:

$$W_x=r_{11}p_x+r_{12}p_y+r_{13}p_z, \tag{11}$$
$$W_y=r_{21}p_x+r_{22}p_y+r_{23}p_z, \tag{12}$$
$$W_z=r_{31}p_x+r_{32}p_y+r_{33}p_z-L_1. \tag{13}$$

From Eqs. (11)–(13), the position of the manipulator's end-jaw can be obtained as:

$$p_x=r_{11}W_x+r_{21}W_y+r_{31}(W_z+L_1)=k_1, \tag{14}$$
$$p_y=r_{12}W_x+r_{22}W_y+r_{32}(W_z+L_1)=k_2, \tag{15}$$
$$p_z=r_{13}W_x+r_{23}W_y+r_{33}(W_z+L_1)=k_3. \tag{16}$$

Substituting Eqs. (14)–(16) into Eq. (10), the following three position-constraint equations can be obtained:

$$k_1=c_1(a_1+a_2c_2+a_3c_{23}+d_4s_{23}-d_6s_{23}c_5-d_6c_{23}c_4s_5)-s_1s_4s_5d_6, \tag{17}$$
$$k_2=s_1(a_1+a_2c_2+a_3c_{23}+d_4s_{23}-d_6s_{23}c_5-d_6c_{23}c_4s_5)+c_1s_4s_5d_6, \tag{18}$$
$$k_3=a_2s_2+a_3s_{23}-d_4c_{23}+c_5c_{23}d_6-c_4s_5s_{23}d_6. \tag{19}$$

Considering that five joint variables (θ_1, θ_2, θ_3, θ_4, and θ_5) are unknown, the joint variables θ_2 and θ_3 are set as the independent variables.

4.1 Solution of joint variable θ_5

By combining Eqs. (17) and (18), a new position-constraint equation can be derived:

$$k_1^2+k_2^2=(a_1+a_2c_2+a_3c_{23}+d_4s_{23}-d_6s_{23}c_5-d_6c_{23}c_4s_5)^2+(s_4s_5d_6)^2. \tag{20}$$

Multiplying both sides of Eq. (20) by s_{23}^2, the following formula can be obtained:

$$s_{23}^2(k_1^2+k_2^2)=\left[(a_1+a_2c_2+a_3c_{23}+d_4s_{23}-d_6s_{23}c_5)\,s_{23}-d_6c_{23}s_{23}c_4s_5\right]^2+(s_{23}s_4s_5d_6)^2. \tag{21}$$

According to Eq. (19), the equations for $s_5s_{23}d_6c_4$ and $s_5s_{23}d_6s_4$ can be derived:

$$s_5s_{23}d_6c_4=a_2s_2+a_3s_{23}-d_4c_{23}+c_5c_{23}d_6-k_3, \tag{22}$$

$$s_5s_{23}d_6s_4=\pm\left[(s_5s_{23}d_6)^2-(a_2s_2+a_3s_{23}-d_4c_{23}+c_5c_{23}d_6-k_3)\right]^2. \tag{23}$$

Substituting Eqs. (22) and (23) into Eq. (21), Eq. (21) can be rewritten as:

$$-2d_6c_5i=s_{23}(k_1^2+k_2^2)-s_{23}i^2+2c_{23}ij+s_{23}j^2-d_6^2s_{23}, \tag{24}$$

$$i=a_1+a_2c_2+a_3c_{23}+d_4s_{23}, \tag{25}$$

$$j=a_2s_2+a_3s_{23}-d_4c_{23}-k_3. \tag{26}$$

4.1.1 Case 1: s_{23}=0

By substituting s_{23}=0 into Eq. (19), Eq. (19) can be rewritten as:

$$k_3=a_2s_2-d_4c_{23}+c_5c_{23}d_6. \tag{27}$$

From Eq. (27), the analytical solution of θ_5 in case 1 can be obtained as:

$$\theta_5=\arccos\left[\frac{k_3-a_2s_2+d_4c_{23}}{c_{23}d_6}\right]. \tag{28}$$

4.1.2 Case 2: $s_{23}\neq0\wedge a_1+a_2c_2+a_3c_{23}+d_4s_{23}\neq0$

From Eq. (24), the analytical solution of θ_5 in case 2 can be obtained as:

$$\theta_5=\arccos\left[-\frac{s_{23}(k_1^2+k_2^2)-s_{23}i^2+2c_{23}ij+s_{23}j^2-d_6^2s_{23}}{2d_6i}\right]. \tag{29}$$

4.1.3 Case 3: $s_{23}\neq0\wedge a_1+a_2c_2+a_3c_{23}+d_4s_{23}=0$

By substituting i=0 into Eq. (24), Eq. (24) can be rewritten as:

$$0=k_1^2+k_2^2-d_6^2+(a_2s_2+a_3s_{23}-d_4c_{23}-k_3)^2. \tag{30}$$

Eq. (30) is not influenced by joint variable θ_5. The analytical solution of θ_5 in case 3 can be obtained as:

$$\theta_5=\forall,\quad \text{if } k_1^2+k_2^2-d_6^2+(a_2s_2+a_3s_{23}-d_4c_{23}-k_3)^2=0. \tag{31}$$

In summary, the analytical solution of θ_5 can be expressed as:

$$\theta_5=\zeta(\theta_2,\,\theta_3)=\begin{cases}\forall, & a_1+a_2c_2+a_3c_{23}+d_4s_{23}=0\wedge s_{23}\neq0\wedge\\ & k_1^2+k_2^2+(a_2s_2+a_3s_{23}-d_4c_{23}-k_3)^2-d_6^2=0,\\ \arccos\left[\dfrac{k_3-a_2s_2+d_4c_{23}}{c_{23}d_6}\right], & s_{23}=0,\\ \arccos\left[-\dfrac{s_{23}(k_1^2+k_2^2)-s_{23}i^2+2c_{23}ij+s_{23}j^2-s_{23}d_6^2}{2d_6i}\right], & a_1+a_2c_2+a_3c_{23}+d_4s_{23}\neq0\wedge s_{23}\neq0.\end{cases} \tag{32}$$

4.2 Solution of joint variable θ_4

Substituting Eq. (32) into Eqs. (17) – (19), the three position-constraint equations can be rewritten as:

$$k_1=c_1\left(a_1+a_2c_2+a_3c_{23}+d_4s_{23}-d_6s_{23}c_\zeta-d_6c_{23}c_4s_\zeta\right)-s_1s_4s_\zeta d_6, \tag{33}$$

$$k_2=s_1\left(a_1+a_2c_2+a_3c_{23}+d_4s_{23}-d_6s_{23}c_\zeta-d_6c_{23}c_4s_\zeta\right)+c_1s_4s_\zeta d_6, \tag{34}$$

$$k_3=a_2s_2+a_3s_{23}-d_4c_{23}+c_\zeta c_{23}d_6-c_4s_\zeta s_{23}d_6, \tag{35}$$

where s_ζ denotes $\sin\zeta$, and c_ζ denotes $\cos\zeta$.

4.2.1 Case 1: $s_\zeta=0$

By substituting $s_\zeta=0$ into Eqs. (33)–(35), the three position-constraint equations can be rewritten as:

$$k_1=c_1(a_1+a_2c_2+a_3c_{23}+d_4s_{23}-d_6s_{23}c_\zeta), \tag{36}$$

$$k_2=s_1(a_1+a_2c_2+a_3c_{23}+d_4s_{23}-d_6s_{23}c_\zeta), \tag{37}$$

$$k_3=a_2s_2+a_3s_{23}-d_4c_{23}+c_\zeta c_{23}d_6. \tag{38}$$

Combining Eqs. (36) and (37), the following formula can be obtained:

$$k_1^2+k_2^2=\left(a_1+a_2c_2+a_3c_{23}+d_4s_{23}-d_6s_{23}c_\zeta\right)^2. \quad (39)$$

Eqs. (38) and (39) are not influenced by joint variable θ_4. The analytical solution of θ_4 in case 1 can be obtained as:

$$\theta_4=\forall, \quad \text{if } k_3=a_2s_2+a_3s_{23}-d_4c_{23}+c_\zeta c_{23}d_6\wedge k_1^2+k_2^2=(a_1+a_2c_2+a_3c_{23}+d_4s_{23}-d_6s_{23}c_5)^2. \quad (40)$$

4.2.2 Case 2: $s_\zeta\neq0\wedge s_{23}=0\wedge a_1+a_2c_2+a_3c_{23}\neq0$

Substituting $s_{23}=0$ into Eqs. (33)–(35), the three position-constraint equations can be rewritten as:

$$k_1=c_1(a_1+a_2c_2+a_3c_{23}-d_6c_{23}c_4s_\zeta)-s_1s_4s_\zeta d_6, \quad (41)$$
$$k_2=s_1(a_1+a_2c_2+a_3c_{23}-d_6c_{23}c_4s_\zeta)+c_1s_4s_\zeta d_6, \quad (42)$$
$$k_3=a_2s_2-d_4c_{23}+c_\zeta c_{23}d_6. \quad (43)$$

Combining Eqs. (41) and (42), the following formula can be obtained:

$$k_1^2+k_2^2=-(a_1+a_2c_2+a_3c_{23})^2-\left(d_6s_\zeta\right)^2-2d_6c_{23}c_4s_\zeta(a_1+a_2c_2+a_3c_{23}). \quad (44)$$

The analytical solution of θ_4 in case 2 can be obtained from Eq. (44) as follows:

$$\theta_4=\arccos\left[-\frac{k_1^2+k_2^2-(a_1+a_2c_2+a_3c_{23})^2-\left(d_6s_\zeta\right)^2}{2d_6c_{23}s_\zeta(a_1+a_2c_2+a_3c_{23})}\right]. \quad (45)$$

4.2.3 Case 3: $s_\zeta\neq0\wedge s_{23}=0\wedge a_1+a_2c_2+a_3c_{23}=0$

Substituting s_{23}=0 and $a_1+a_2c_2+a_3c_{23}=0$ into Eqs. (33)–(35), the three position-constraint equations can be rewritten as:

$$k_1=-c_1c_{23}c_4s_\zeta d_6-s_1s_4s_\zeta d_6, \quad (46)$$
$$k_2=-s_1c_{23}c_4s_\zeta d_6+c_1s_4s_\zeta d_6, \quad (47)$$
$$k_3=a_2s_2-d_4c_{23}+c_\zeta c_{23}d_6. \quad (48)$$

Combining Eqs. (46) and (47), the following formula can be obtained:

$$k_1^2+k_2^2=\left(d_6s_\zeta\right)^2. \quad (49)$$

According to Eq. (49), joint variable θ_4 has no effect on Eq. (49). The analytical solution of θ_4 in case 3 can be obtained as:

$$\theta_4=\forall, \quad \text{if } k_1^2+k_2^2=\left(d_6s_\zeta\right)^2. \quad (50)$$

4.2.4 Case 4: $s_\zeta\neq0\wedge s_{23}\neq0$

From Eq. (35), the analytical solution of θ_4 in case 4 can be obtained as:

$$\theta_4=\arccos\left[\frac{a_2s_2+a_3s_{23}-d_4c_{23}+c_\zeta c_{23}d_6-k_3}{s_\zeta s_{23}d_6}\right]. \quad (51)$$

In summary, the analytical solution of θ_4 can be expressed as:

$$\theta_4=\eta(\theta_2,\ \theta_3,\ \zeta)=\begin{cases}\forall, & s_\zeta=0\wedge k_3=a_2s_2+a_3s_{23}-d_4c_{23}+c_\zeta c_{23}d_6\wedge\\ & k_1^2+k_2^2=\left(a_1+a_2c_2+a_3c_{23}+d_4s_{23}-d_6s_{23}c_\zeta\right)^2,\\ \forall, & s_\zeta\neq0\wedge s_{23}=0\wedge a_1+a_2c_2+a_3c_{23}=0\wedge\\ & k_1^2+k_2^2=\left(d_6s_\zeta\right)^2,\\ \arccos\left[-\dfrac{k_1^2+k_2^2-(a_1+a_2c_2+a_3c_{23})^2-\left(d_6s_\zeta\right)^2}{2d_6c_{23}s_\zeta(a_1+a_2c_2+a_3c_{23})}\right], & s_\zeta\neq0\wedge s_{23}=0\wedge a_1+a_2c_2+a_3c_{23}\neq0,\\ \arccos\left[\dfrac{a_2s_2+a_3s_{23}-d_4c_{23}+c_\zeta c_{23}d_6-k_3}{s_\zeta s_{23}d_6}\right], & s_\zeta\neq0\wedge s_{23}\neq0.\end{cases} \quad (52)$$

4.3 Solution of joint variable θ_1

Substituting the results obtained from Eqs. (32) and (52) into Eqs. (17) and (18), Eqs. (17) and (18) can be rewritten as:

$$k_1=c_1w_y-s_1w_x, \quad (53)$$
$$k_2=s_1w_y+c_1w_x, \quad (54)$$
$$w_x=s_\eta s_\zeta d_6, \quad (55)$$
$$w_y=a_1+a_2c_2+a_3c_{23}+d_4s_{23}-d_6s_{23}c_\zeta-d_6c_{23}c_\eta s_\zeta, \quad (56)$$

where s_η denotes $\sin\eta$, and c_η denotes $\cos\eta$.

4.3.1 Case 1: $w_x\neq0\vee w_y\neq0$

Eqs. (53) and (54) can be rewritten as:

$$\sqrt{w_x^2+w_y^2}\sin\left[\text{Atan2}\left(w_y,\ w_x\right)-\theta_1\right]=k_1, \quad (57)$$

$$\sqrt{w_x^2+w_y^2}\cos\left[\text{Atan2}\left(w_y,\ w_x\right)-\theta_1\right]=k_2. \quad (58)$$

From Eqs. (57) and (58), the analytical solution of θ_1 in case 1 can be obtained as:

$$\theta_1=\text{Atan2}\left(w_y,\ w_x\right)-\text{Atan2}\left(k_1,\ k_2\right). \quad (59)$$

4.3.2 Case 2: $w_x=0\wedge w_y=0$

By substituting $w_x=0$ and $w_y=0$ into Eqs. (53) and (54), Eqs. (53) and (54) can be rewritten as:

$$k_1=0, \quad (60)$$

$$k_2=0. \quad (61)$$

According to Eqs. (60) and (61), joint variable θ_1 has no effect on the x-position or y-position of the manipulator's end-jaw. The analytical solution of θ_1 in case 2 can be obtained as:

$$\theta_1=\forall. \quad (62)$$

In summary, the analytical solution of θ_1 can be expressed as:

$$\theta_1=\gamma\left(\theta_2,\ \theta_3,\ \zeta,\ \eta\right)=\begin{cases}\forall, & w_x=0\wedge w_y=0,\\ \text{Atan2}\left(w_y,\ w_x\right)-\text{Atan2}\left(k_1,\ k_2\right), & w_x\neq0\vee w_y\neq0.\end{cases} \quad (63)$$

4.4 Model verification

Table S1 in the electronic supplementary materials (ESM) depicts the key points of desired core-drilling trajectory A, the calculated joint trajectory, and the resulted core-drilling-tip trajectory. The calculated joint trajectory is determined based on the desired core-drilling trajectory A by means of the established double-redundancy inverse kinematic model. The resulted core-drilling-tip trajectory is resolved according to the calculated joint trajectory (the calculated θ_1–θ_6 in Table S1) by means of the established core-drilling forward kinematic model presented in Section 3. As can be seen from Table S1, high consistency between desired core-drilling trajectory A and the resulted core-drilling-tip trajectory is observed. Trajectory A can also be fulfilled by other joint trajectories (θ_1, θ_4, θ_5, and θ_6) if θ_2 and θ_3 are preset to be different values. Hence, the established double-redundancy inverse kinematic model is effective for solving the trajectories of six active joints according to desired core-drilling trajectory.

5 Case study

The core-drilling workspaces and the core-drilling trajectories of Jiaolong submersible manipulator are simulated and analyzed in this section. The mechanical parameters of the manipulator are depicted in Table 1. The length of the core-drilling rig L_1 was set as 620 mm.

Table 1 Parameters of the Jiaolong submersible manipulator

i	a_{i-1} (mm)	α_{i-1}	d_i (mm)	θ_i	Range of joint variable θ_i
1	–	0°	–	θ_1	−60.0°–60.0°
2	69.9	90°	–	θ_2	−32.0°–90.0°
3	894.3	0°	–	θ_3	−88.1°–44.9°
4	135.4	90°	500.6	θ_4	−135.0°–135.0°
5	–	−90°	–	θ_5	154.0°–274.0°
6	–	−90°	412.0	θ_6	−180.0°–180.0°

5.1 Core-drilling workspace analysis

Using the established core-drilling forward kinematic model, we simulated the core-drilling workspace of the Jiaolong submersible without incline and rotation (yaw angle α=0°, pitch angle β=0°, and roll angle γ=0°), as shown in Fig. 3. While calculating the core-drilling points within the workspace, each joint variable was defined by 20 points evenly spaced throughout the range (resulting in 3.2×10^6 discrete working points across the workspace). The 3D view of the core-drilling workspace of the Jiaolong submersible manipulator in the w-coordinate is depicted in Fig. 3a. The x-y, x-z, and y-z views of the core-drilling workspace in the w-coordinate are shown in Figs. 3b–3d, respectively. The core-drilling workspace surrounds the manipulator, the envelope surface of which is like an ellipsoid. The reachable core-drilling motion range was: −300.5–1847.0 mm in the x direction, −1656.6–1656.6 mm in the y direction, and −2023.7–1133.9 mm in the z direction.

The core-drilling workspace of the inclined Jiaolong submersible manipulator was further analyzed, as shown in Fig. 4. We simulated 3.2×10^6 discrete working points within the core-drilling workspace by

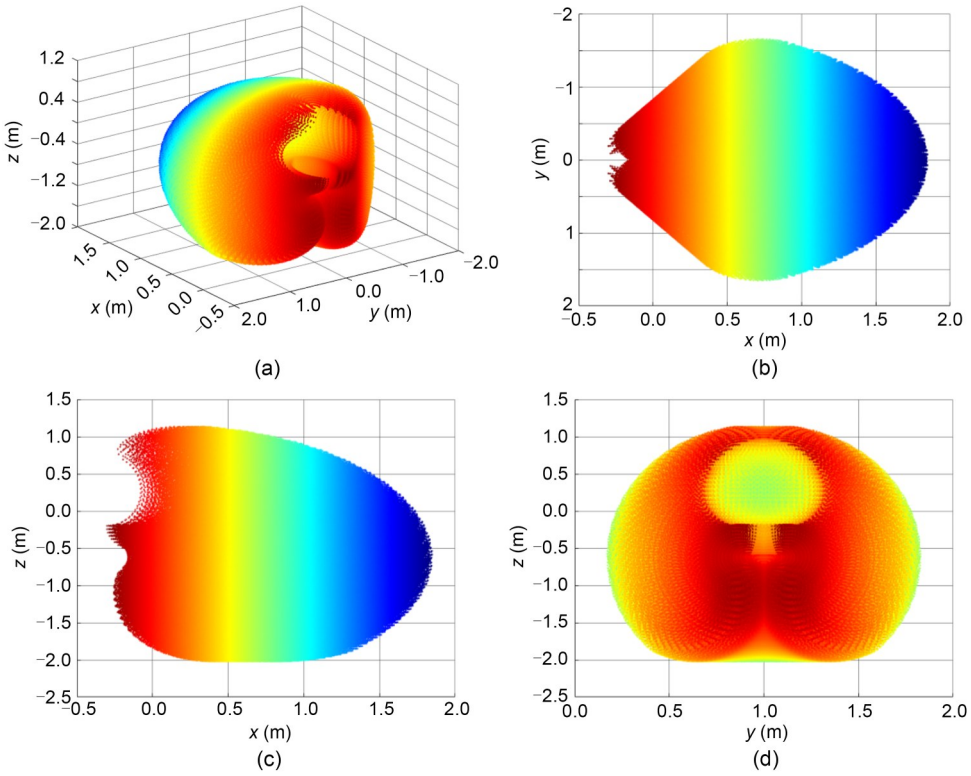

Fig. 3 Core-drilling workspace of the Jiaolong submersible manipulator without incline and rotation (α=0°, β=0°, and γ=0°): (a) 3D view; (b) *x*-*y* view; (c) *x*-*z* view; (d) *y*-*z* view

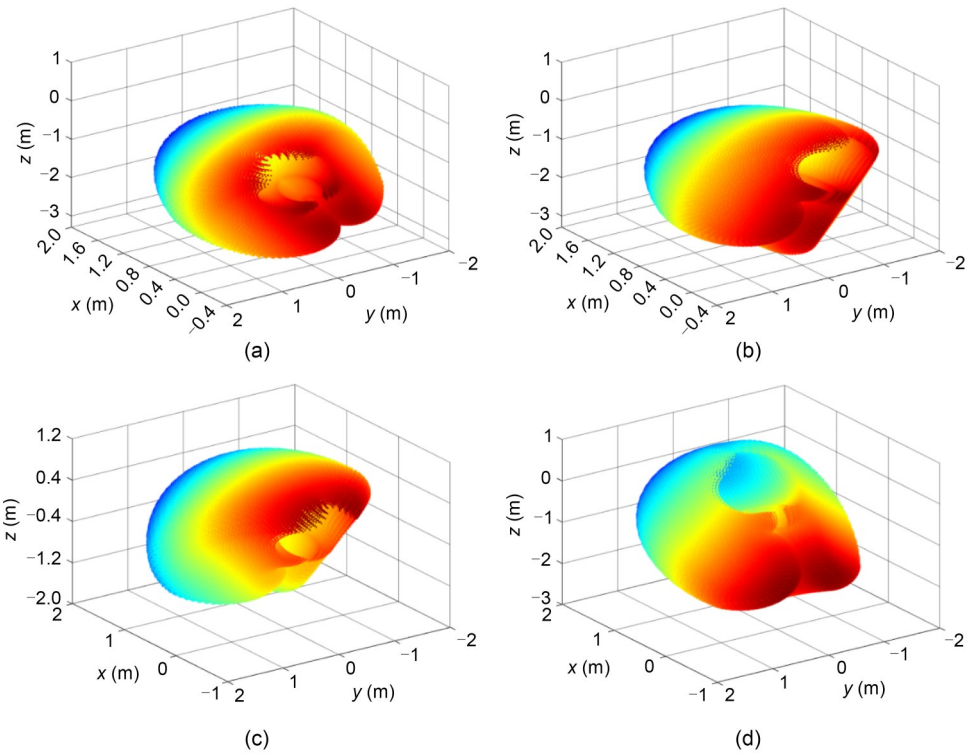

Fig. 4 Core-drilling workspace of the Jiaolong submersible manipulator with different postures: (a) α=0°, β=0°, and γ=−30°; (b) α=0°, β=0°, and γ=30°; (c) α=0°, β=−30°, and γ=0°; (d) α=0°, β=30°, and γ=0°

setting each joint variable to be 20 equally spaced points within its range. Fig. 4a depicts the core-drilling workspace of the Jiaolong submersible manipulator with roll angle γ of −30° in the w-coordinate. While roll angle γ is set to be 30°, the core-drilling workspace of the Jiaolong submersible manipulator is shown in Fig. 4b. While pitch angle β is set to be −30°, the core-drilling workspace of the Jiaolong submersible manipulator is shown in Fig. 4c. While the pitch angle β is set to be 30°, the core-drilling workspace of the Jiaolong submersible manipulator is shown in Fig. 4d. It is clear from the figure that the core-drilling workspace is influenced by the posture of the Jiaolong submersible. Therefore, the submersible posture is a significant factor for deep-sea core drilling.

5.2 Core-drilling trajectory analysis

Based on the double-redundancy inverse kinematic model of the Jiaolong submersible manipulator, we simulated and analyzed the core-drilling joint trajectories. As shown in Fig. 5, we designed a core-drilling trajectory A (start point: (1000, 0, −900) mm; end point: (1000, 0, −1200) mm). Trajectory A could be executed by forcing the six active rotational joints of the manipulator to move along the designed joint trajectory. When θ_2 and θ_3 were preset (according to the established core-drilling inverse kinematic model in Section 4, joint variables θ_2 and θ_3 are independent variables which should be set before inverse kinematic calculation), the four joint trajectories (θ_1, θ_4, θ_5, and θ_6) of Jiaolong submersible manipulator could be determined. Fig. 6 depicts the required joint trajectories for core-drilling trajectory A when the Jiaolong submersible was in a horizontal posture with α=0°, β=0°, and γ=0° and in an incline posture with α=0°, β=10°, and γ=10°.

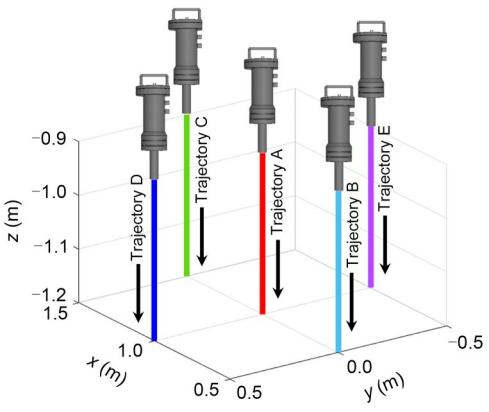

Fig. 5 Core-drilling trajectories A, B, C, D, and E

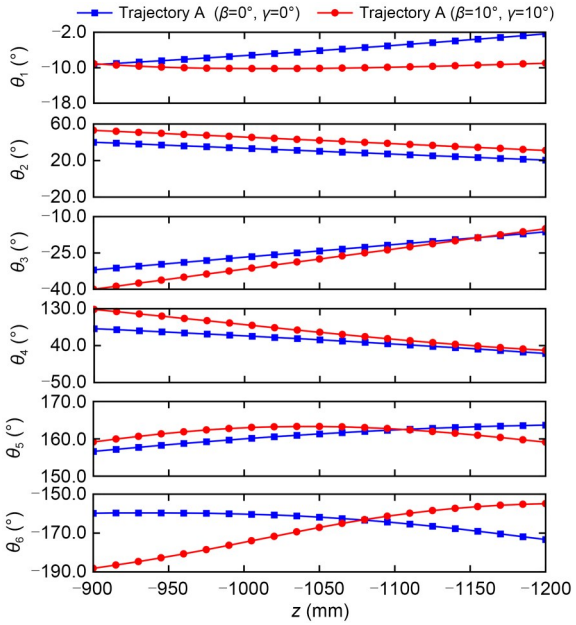

Fig. 6 Six joint variables (θ_1, θ_2, θ_3, θ_4, θ_5, and θ_6) of core-drilling trajectory A with Jiaolong submersible manipulator in two different postures

In addition, we designed another four core-drilling trajectories: trajectory B (start point: (500, 0, −900) mm; end point: (500, 0, −1200) mm), trajectory C (start point: (1500, 0, −900) mm; end point: (1500, 0, −1200) mm), trajectory D (start point: (1000, 500, −900) mm; end point: (1000, 500, −1200) mm), and trajectory E (start point: (1000, −500, −900) mm; end point: (1000, −500, −1200) mm), as shown in Fig. 5. We solved the six joint trajectories of the manipulator for the four core-drilling trajectories, as depicted in Fig 7. Therefore, the double-redundancy inverse kinematic model is computationally effective.

6 Conclusions

This paper proposed a core-drilling kinematic model for the Jiaolong submersible manipulator, comprised of two key parts: forward kinematics and inverse kinematics. Based on the established kinematic model, several numerical examples corresponding to the core-drilling tasks under different submersible postures were carried out. Three main conclusions can be drawn:

(1) The core-drilling posture (along the gravitational direction) of the Jiaolong submersible manipulator can be guaranteed by regulating the sixth active joint according to the other five active joints of the

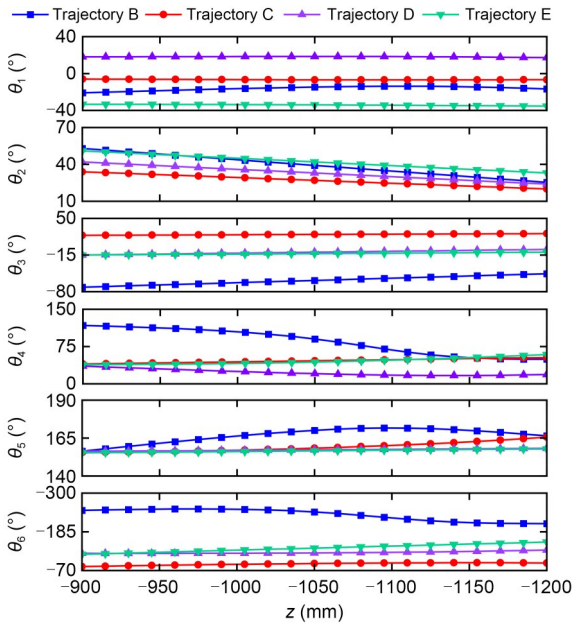

Fig. 7 Six joint variables (θ_1, θ_2, θ_3, θ_4, θ_5, and θ_6) of core-drilling trajectories B, C, D, and E with Jiaolong submersible manipulator at α=0°, β=10°, and γ=10°

manipulator and the posture of the Jiaolong submersible. Herein, the core-drilling forward kinematics of Jiaolong submersible manipulator involves five independent variables.

(2) The core-drilling trajectory can be realized by enforcing the first, fourth, and fifth active joints along the solved trajectories while the second and third active joints are in preset positions. Meanwhile, the sixth active joint should be regulated to assure a constant core-drilling posture.

(3) The Jiaolong submersible manipulator is able to perform core-drilling task in an ellipsoid workspace with an x-directional range of −300.5–1847.0 mm, a y-directional range of −1656.6–1656.6 mm, and a z-directional range of −2023.7–1133.9 mm (in the w-coordinate) while the submersible is without incline and rotation.

Acknowledgments

This work is supported by the National Natural Science Foundation of China (No. 52175018) and the Key R&D Program of Shandong Province (Major Scientific and Technological Innovation Project) (No. 2019JZZY010802), China.

Author contributions

Xu YANG and Xin LIU designed the research and processed the corresponding data. Yugang REN, Shizhen LI, and Limin ZHU wrote the first draft of the manuscript. Xu YANG and Xin LIU organized the manuscript. Xu YANG, Shizhen LI, and Yugang REN revised and edited the final version.

Conflict of interest

Xu YANG, Xin LIU, Shizhen LI, Yugang REN, and Limin ZHU declare that they have no conflict of interest.

References

Chen P, Long JC, Yang W, et al., 2021. Inverse kinematics solution of underwater manipulator based on Jacobi matrix. OCEANS 2021: San Diego–Porto, p.1-4. https://doi.org/10.23919/OCEANS44145.2021.9705690

Chu FY, Qian XY, Zhang HS, et al., 2005. Discovery of ferromanganese crust boundary and its genetic and ore prospecting significance. *Journal of Zhejiang University SCIENCE*, 6(7):656-662. https://doi.org/10.1631/jzus.2005.A0656

Cui WC, 2013. Development of the Jiaolong deep manned submersible. *Marine Technology Society Journal*, 47(3): 37-54. https://doi.org/10.4031/MTSJ.47.3.2

Dereli S, Köker R, 2020. A meta-heuristic proposal for inverse kinematics solution of 7-DOF serial robotic manipulator: quantum behaved particle swarm algorithm. *Artificial Intelligence Review*, 53(2):949-964. https://doi.org/10.1007/s10462-019-09683-x

Iizasa K, Fiske RS, Ishizuka O, et al., 1999. A Kuroko-type polymetallic sulfide deposit in a submarine silicic caldera. *Science*, 283(5404):975-977. https://doi.org/10.1126/science.283.5404.975

Khan A, Quan WL, 2015. Forward kinematic modeling and analysis of 6-DOF underwater manipulator. International Conference on Fluid Power and Mechatronics, p.1093-1096. https://doi.org/10.1109/FPM.2015.7337281

Khlystov O, de Batist M, Shoji H, et al., 2013. Gas hydrate of Lake Baikal: discovery and varieties. *Journal of Asian Earth Sciences*, 62:162-166. https://doi.org/10.1016/j.jseaes.2012.03.009

Kohnen W, 2013. Review of deep ocean manned submersible activity in 2013. *Marine Technology Society Journal*, 47(5): 56-68. https://doi.org/10.4031/MTSJ.47.5.6

Kohnen W, 2018. MTS manned underwater vehicles 2017-2018 global industry overview. *Marine Technology Society Journal*, 52(5):125-151. https://doi.org/10.4031/MTSJ.52.5.9

Lauro FM, McDougald D, Thomas T, et al., 2009. The genomic basis of trophic strategy in marine bacteria. *Proceedings of the National Academy of Sciences of the United States of America*, 106(37):15527-15533. https://doi.org/10.1073/pnas.0903507106

Li GF, Xiao F, Zhang XF, et al., 2022. An inverse kinematics method for robots after geometric parameters compensation. *Mechanism and Machine Theory*, 174:104903. https://doi.org/10.1016/j.mechmachtheory.2022.104903

Li LY, Li X, Zhou X, et al., 2007. Study of off-line programming

system of arc robot based on the software of ROBOGUIDE. *In*: Tarn TJ, Chen SB, Zhou CJ (Eds.), Robotic Welding, Intelligence and Automation. Springer, Berlin, Germany, p.401-408. https://doi.org/10.1007/978-3-540-73374-4_48

Liu F, Cui WC, Li XY, 2010. China's first deep manned submersible, JIAOLONG. *Science China Earth Sciences*, 53(10):1407-1410. https://doi.org/10.1007/s11430-010-4100-2

Luo S, Chu DM, Li QD, et al., 2022. Inverse kinematics solution of 6-DOF manipulator based on multi-objective full-parameter optimization PSO algorithm. *Frontiers in Neurorobotics*, 16:791796. https://doi.org/10.3389/fnbot.2022.791796

Qiao SG, Liao QZ, Wei SM, et al., 2010. Inverse kinematic analysis of the general 6R serial manipulators based on double quaternions. *Mechanism and Machine Theory*, 45(2): 193-199. https://doi.org/10.1016/j.mechmachtheory.2009.05.013

Ravilly M, Horen H, Perrin M, et al., 2001. NRM intensity of altered oceanic basalts across the MAR (21°N, 0–1.5 Ma): a record of geomagnetic palaeointensity variations? *Geophysical Journal International*, 145(2):401-422. https://doi.org/10.1046/j.1365-246x.2001.01381.x

Reagan MK, Pearce JA, Petronotis K, et al., 2017. Subduction initiation and ophiolite crust: new insights from IODP drilling. *International Geology Review*, 59(11):1439-1450. https://doi.org/10.1080/00206814.2016.1276482

Ren YG, Yang L, Liu YJ, et al., 2021. Experimental research on the process parameters of a novel low-load drill bit used for 7000 m bedrock sampling base on manned submersible. *Journal of Marine Science and Engineering*, 9(6): 682. https://doi.org/10.3390/jmse9060682

Roh HS, Kim JO, 2004. Manipulator modeling from D-H parameters. The 30th Annual Conference of IEEE Industrial Electronics Society, p.2480-2485. https://doi.org/10.1109/IECON.2004.1432190

Sivčev S, Coleman J, Omerdić E, et al., 2018. Underwater manipulators: a review. *Ocean Engineering*, 163:431-450. https://doi.org/10.1016/j.oceaneng.2018.06.018

Stakes D, Moore WS, Tengdin T, et al., 1992. Cores drilled into active smokers on Juan de Fuca Ridge. *Eos, Transactions American Geophysical Union*, 73(26):273-283. https://doi.org/10.1029/91EO00220

Tsuchiya M, Nomaki H, Kitahashi T, et al., 2019. Sediment sampling with a core sampler equipped with aluminum tubes and an onboard processing protocol to avoid plastic contamination. *MethodsX*, 6:2662-2668. https://doi.org/10.1016/j.mex.2019.10.027

Wang D, Wu J, Wang LP, 2018. Research on the error transfer characteristics of a 3-DOF parallel tool head. *Robotics and Computer-Integrated Manufacturing*, 50:266-275. https://doi.org/10.1016/j.rcim.2017.10.002

Wang WZ, Zhang SS, Ye C, et al., 2020. A new method for optimizing the cabin layout of manned submersibles. *Complexity*, 2020:6626602. https://doi.org/10.1155/2020/6626602

Wu SJ, Yang CJ, Huang HC, et al., 2014. Development of an electric control gas-tight sampler for seafloor hydrothermal fluids. *Journal of Zhejiang University-SCIENCE A (Applied Physics & Engineering)*, 15(2):120-129. https://doi.org/10.1631/jzus.A1300233

Xiao F, Li GF, Jiang D, et al., 2021. An effective and unified method to derive the inverse kinematics formulas of general six-DOF manipulator with simple geometry. *Mechanism and Machine Theory*, 159:104265. https://doi.org/10.1016/j.mechmachtheory.2021.104265

Yao HQ, Liu YG, Yang Y, et al., 2021. Assessment of acoustic backscatter intensity surveying on deep-sea ferromanganese crust: constraints from Weijia Guyot, western Pacific Ocean. *China Geology*, 4(2):288-298. https://doi.org/10.31035/cg2020046

Zhang J, Li W, Yu JC, et al., 2017. Study of manipulator operations maneuvered by a ROV in virtual environments. *Ocean Engineering*, 142:292-302. https://doi.org/10.1016/j.oceaneng.2017.07.008

Zhang TW, Ding ZJ, Zhao SY, et al., 2016. Positioning sonars of Jiaolong human occupied vehicle: basic principle and sea trial. OCEANS 2016–Shanghai, p.1-4. https://doi.org/10.1109/OCEANSAP.2016.7485336

Zhang TW, Tang JL, Li ZG, et al., 2018. Use of the Jiaolong manned submersible for accurate mapping of deep-sea topography and geomorphology. *Science China Earth Sciences*, 61(8):1148-1156. https://doi.org/10.1007/s11430-017-9187-3

Zhang Y, Li XH, Yu TT, et al., 2022. Trajectory planning of deep-sea hydraulic manipulator in joint space with flow constraints. International Symposium on Control Engineering and Robotics, p.31-37. https://doi.org/10.1109/ISCER55570.2022.00012

Zhu M, 2020. Acoustic system of Jiaolong manned submersible and its future development. *In*: Chinese Academy of Sciences, Cyberspace Administration of China, Ministry of Education of the PRC, et al. (Eds.), China's e-Science Blue Book 2018. Springer, Singapore, p.171-186. https://doi.org/10.1007/978-981-13-9390-7_9

Electronic supplementary materials

Table S1